Schweizerischer Erdbebendienst
Service Sismologique Suisse
Servizio Sismico Svizzero
Servizi da Terratrembels Svizzer

ETH
Eidgenössische Technische Hochschule Zürich
Swiss Federal Institute of Technology Zurich

St Gallen - Klosterhof (STGK)

SITE CHARACTERIZATION REPORT

Clotaire MICHEL, Jan BURJANEK, Carlo CAUZZI

Daniel ROTEN, Valerio POGGI, Donat FÄH

Sonneggstrasse 5 CH-8092 Zürich Switzerland; E-mail: clotaire.michel@sed.ethz.ch

Last modified : October 17, 2013

Abstract

Ambient vibration array measurements were performed in the old city centre of St Gallen in order to characterize the velocity profile under the new station STGK of the Swiss Strong Motion Network (SSMNet). Two array configurations were performed up to $160\,\mathrm{m}$ aperture. Basic assumptions of array analysis were not fulfilled, including a strong lateral variability. Especially, ellipticity information was not robust enough to constrain the inversion. However, the results agree with borehole data and the observations of earthquakes at the STGK stations are consistent as well. The fundamental frequency at STGK station is $4\,\mathrm{Hz}$. Moreover, a H/V survey allowed to map the fundamental frequency below St Gallen city. Because of the lateral variability of the different layers, interpreting this frequency in terms of bedrock depth is however difficult. At STGK site, $V_{s,30}$ is found to be close to $440\,\mathrm{m/s}$, and the site class is B in EC8 and E in SIA261. The theoretical SH transfer function and impedance contrast of the quarter-wavelength velocity computed from the inverted profiles support a large amplification above $5\,\mathrm{Hz}$.

Contents

1 Introduction

The station STGK (St Gallen Klosterhof) is part of the Swiss Strong Motion Network (SSMNet) in Eastern Switzerland. STGK is a new site installed in the framework of the SSMNet Renewal project in 2012. It was installed before the start of the deep geothermal project and therefore recorded ground motion of induced earthquakes in the city. The renewal project includes also the site characterization. Passive array measurement has been selected as a standard tool to investigate these sites. Such a measurement campaign was performed on 14th March 2012 around the monastery of Gallus (Klosterhof) in St Gallen (Fig. 1), with a centre $75\,\mathrm{m}$ SW from the station STGK, in order to characterize the sediments under this station. According to the geological map, this station is located on moraine (Würm) on top of Miocene (Langhian-Serravallian) Molasse rock (sandstone and marls). Archeological work and boreholes showed that moraine does not reach the surface and can be found at very variable depths in this area. An additional H/V survey was performed in the city between November 13th and 20th 2010 by I. Egger and on May 18th by A. Stutz. This report presents the measurement setups, the results of the H/V analysis and of the array processing of surface waves (dispersion curves). Then, an inversion of these results for a velocity profile is performed. Standard parameters are derived to evaluate the amplification at this site.

Canton	**City**	**Location**	**Station code**	**Site type**	**Slope**
St Gallen	St Gallen	Klosterhof	STGK	Moraine	Slight slope

Table 1: Main characteristics of the study-site.

Figure 1: Picture of the site.

2 Experiment description

2.1 Ambient Vibrations

The ground surface is permanently subjected to ambient vibrations due to:

- natural sources (ocean and large-scale atmospheric phenomena) below $1\,\mathrm{Hz}$,
- local meteorological conditions (wind and rain) at frequencies around $1\,\mathrm{Hz}$,
- human activities (industrial machines, traffic...) at frequencies above $1\,\mathrm{Hz}$ [Bonnefoy-Claudet et al., 2006].

The objective of the measurements is to record these ambient vibrations and to use their propagation properties to infer the underground structure. First, the polarization of the recorded waves (H/V ratio) is used to derive the resonance frequencies of the soil column. Second, the arrival time delays at many different stations are used to derive the velocity of surface waves at different frequencies (dispersion). The information (H/V, dispersion curves) is then used to derive the properties of the soil column using an inversion process.

2.2 Equipment

For the array measurements 10 Quanterra Q330 dataloggers named NR01 to NR12 (except NR09 and NR11) and 14 Lennartz 3C 5 s seismometers were available (see Tab. 2). Each datalogger can record on 2 ports A (channels EH1, EH2, EH3 for Z, N, E directions) and B (channels EH4, EH5, EH6 for Z, N, E directions). The time synchronization was ensured by GPS. The sensors are placed on a metal tripod directly on the ground. Some points were located on the grass with a weak coupling as it was not allowed to dig holes.

For the single station measurements, a Nanometrics Taurus with a Lennartz 3C 5 s seismometer was used for the first campaign. A laptop with a seedlink server could be linked to the datalogger and stream the data. They could therefore be read by the Geopsy software `http://www.geopsy.org` and the processing made near real-time. It allowed therefore to have an idea of the results directly on the field, refine the measurement grid where it was necessary, record more time if necessary etc. However, problems in the acquisition chain (Taurus/Lennartz) were noticed, so that a Q330 and Lennartz 3C 5 s seismometer were used for the second campaign. The time stamps were not always synchronized on GPS and may suffer from a shift of several seconds. The sensor is placed directly on the ground (generally road) and leveled using the screws.

2.3 Geometry of the arrays

Two array configurations were used, for a total of 4 rings of 10, 20, 40 and $80\,\mathrm{m}$ radius around a central station. The first configuration includes the 3 inner rings with 14 sensors; the second configuration includes the 2 outer rings with 11 sensors. The minimum inter-station distance

Campaign	Digitizer	Model	Number	Resolution
Array		Quanterra Q330	10	24 bits
H/V camp. 1		Nanometrics Taurus	1	24 bits
H/V camp. 2		Quanterra Q330	1	24 bits
Campaign	**Sensor type**	**Model**	**Number**	**Cut-off frequency**
Array	Velocimeter	Lennartz 3C	14	0.2 Hz
H/V camp. 1	Velocimeter	Lennartz 3C	1	0.2 Hz
H/V camp. 2	Velocimeter	Lennartz 3C	1	0.2 Hz

Table 2: Equipment used for the different field campaigns.

and the aperture are therefore 10 and 80 m and 40 and 160 m, respectively. The experimental setup is displayed in Fig. 2. The final usable datasets are detailed in section 3.2.

For the single station measurements, a grid of 30 points (21+9) in the basin including the edges were recorded Fig. 3. The final usable datasets are detailed in section 3.2.

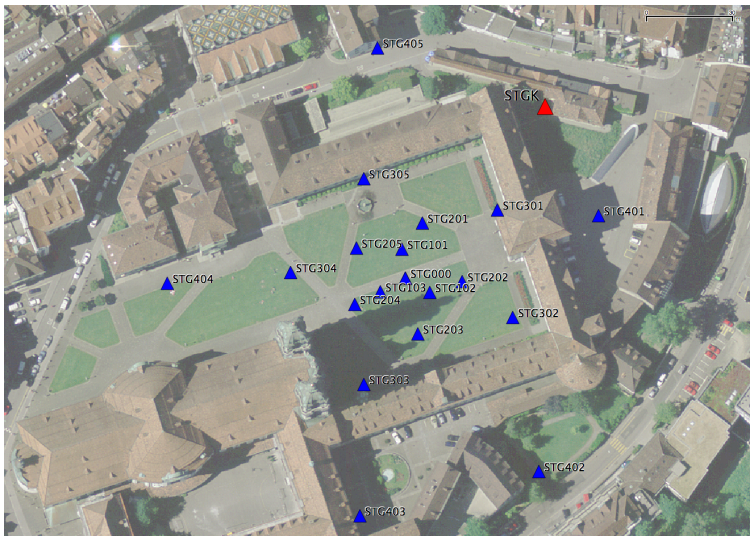

Figure 2: Geometry of the arrays.

2.4 Positioning of the stations

The sensor coordinates of the array were measured using a differential GPS device (Leica Viva), including only a rover station and using the Real Time Kinematic technique provided by Swisstopo. It allows an absolute positioning with an accuracy of about 3 cm on the Swissgrid. This accuracy could not be reached at points STG301 (12 cm), STG303 (10 cm) and STG402 (10 cm), due to the surrounding buildings. These values remain however reasonable for array processing.

For the single station measurements, the positioning of the stations was done by picking points on the 1/25000 Swisstopo map. It allowed a positioning with an accuracy of about 5 m.

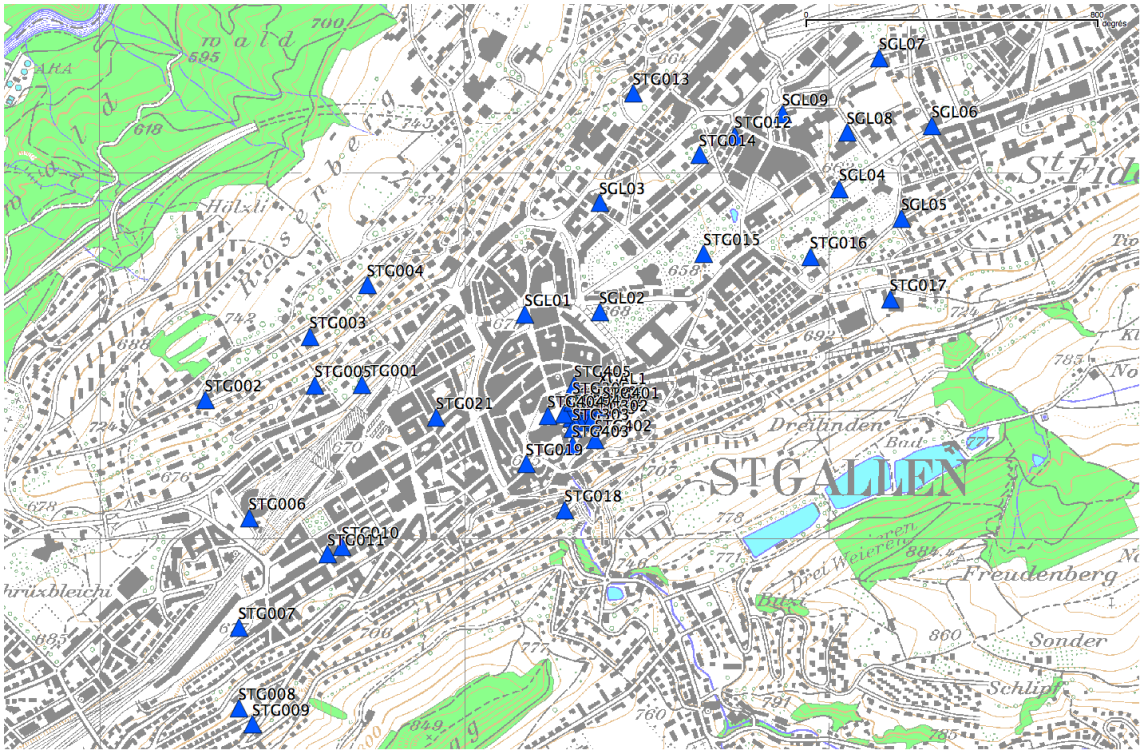

Figure 3: Recorded points in the whole city used for the H/V analysis.

3 Data quality

3.1 Usable data

The largest time windows were extracted, for which all the sensors of the array were in position and the GPS synchronization was ensured (array). Quality of time for station NR07 (point STG403) was lower for the 45 first minutes of dataset 2). An unexplained problem of the Baler of station NR08 induced the lost of 40 min of data for one station connected to 2 sensors, including the central point in the first dataset (problem identified and solved for the second dataset).

GPS measurement were not performed during the datasets to avoid additional noise. A very limited number of vehicles crossed the array (pedestrian zone). However a lot of pedestrians were present due to the nice weather conditions, lying on the grass close to the sensors. Several sources of noise can be recognized on the spectra. First of all, the pedestrians can be seen especially on points STG000, STG405, STG304, STG103 etc. with a broad peak around $2\,\mathrm{Hz}$ especially in the vertical direction for these sensors close to walking paths [Brownjohn et al., 2004]. Points STG203, STG304 show higher noise values at low frequency probably due to bad coupling with the soil (grass). A disturbance with low amplitudes at $1.27\,\mathrm{Hz}$ can be seen on most recordings (3 directions). Then several peaks at different frequencies can be related to surrounding buildings: in STG303, STG301 at $2.9\,\mathrm{Hz}$, in point STG305 at $4\,\mathrm{Hz}$ (peak and filtering of frequencies above) or point STG405 at $3.74\,\mathrm{Hz}$ (very large). More generally, the buildings around the Klosterhof are probably resonating between 2.5 and $4\,\mathrm{Hz}$. Large undamped peaks from machineries can also be seen at 4.79 and $6.55\,\mathrm{Hz}$ in dataset 2.

Orientation of the sensor was checked for the first dataset by maximizing the correlation with the central station. Deviation of $15\,^\circ$ was found for STG303 and STG304 and $\pm 10\,^\circ$ at points STG103 and STG301, lower at the other points. Original and rotated datasets are available for the array analysis.

For the single station measurements, the largest time windows were extracted, for which the sensor was recording in the desired place. For the first campaign, the recordings are not usable below $1\,\mathrm{Hz}$, because of an issue in the acquisition chain (poorly understood Taurus/Lennartz issue).

The characteristics of the datasets are detailed in Tab. 3.

3.2 Data processing

The data were first converted to SAC format including in the header the coordinates of the point (CH1903 system), the recording component and a name related to the position. The name is made of 3 letters characterizing the location (STG here - SGL for the second campaign of single station measurements), 1 digit for the ring and 2 more digits for the number in the ring (array). The response of the sensor was not corrected and the values (in counts) were not converted to $\mathrm{m/s}$.

Dataset	Starting Date	Time	Length	F_s	Min. inter-distance	Aperture	# of points
1	2012/03/14	10:59	72 min	200 Hz	10 m	80 m	14
1_12pts	2012/03/14	10:19	112 min	200 Hz	10 m	80 m	12
2	2012/03/14	13:03	128 min	200 Hz	40 m	160 m	11
Camp1							
STG001	2010/11/13	07:12	30 min	200 Hz			1
STG002	2010/11/13	08:17	30 min	200 Hz			1
STG003	2010/11/13	09:07	31 min	200 Hz			1
STG004	2010/11/13	09:48	29 min	200 Hz			1
STG005	2010/11/13	10:33	30 min	200 Hz			1
STG006	2010/11/13	11:17	31 min	200 Hz			1
STG007	2010/11/13	12:01	30 min	200 Hz			1
STG008	2010/11/13	12:51	30 min	200 Hz			1
STG009	2010/11/13	13:36	30 min	200 Hz			1
STG010	2010/11/13	14:30	8 min	200 Hz			1
STG011	2010/11/13	14:48	30 min	200 Hz			1
STG012	2010/11/20	08:26	31 min	200 Hz			1
STG013	2010/11/20	09:18	30 min	200 Hz			1
STG014	2010/11/20	10:00	30 min	200 Hz			1
STG015	2010/11/20	10:43	30 min	200 Hz			1
STG016	2010/11/20	11:26	30 min	200 Hz			1
STG017	2010/11/20	12:14	30 min	200 Hz			1
STG018	2010/11/20	13:11	30 min	200 Hz			1
STG019	2010/11/20	13:53	30 min	200 Hz			1
STG020	2010/11/20	14:34	29 min	200 Hz			1
STG021	2010/11/20	15:21	28 min	200 Hz			1
Camp2							
SGL01	2011/05/18	07:51	30 min	200 Hz			1
SGL02	2011/05/18	08:44	31 min	200 Hz			1
SGL03	2011/05/18	09:36	28 min	200 Hz			1
SGL04	2011/05/18	10:17	24 min	200 Hz			1
SGL05	2011/05/18	10:55	29 min	200 Hz			1
SGL06	2011/05/18	11:47	29 min	200 Hz			1
SGL07	2011/05/18	13:10	26 min	200 Hz			1
SGL08	2011/05/18	12:31	24 min	200 Hz			1
SGL09	2011/05/18	13:49	29 min	200 Hz			1

Table 3: Usable datasets.

4 H/V processing

4.1 Processing method and parameters

In order to process the H/V spectral ratios, several codes and methods were used. The classical H/V method was computed using the Geopsy `http://www.geopsy.org` software. It averages the ratio of the smoothed Fourier Transform of selected time windows. Tukey windows (cosine taper of 5% width) of $50\,\mathrm{s}$ long overlapping by 50% were selected. Konno and Ohmachi [1998] smoothing procedure with b=60 was used. The classical method computed using the method of Fäh et al. [2001] was also performed.

Moreover, the time-frequency analysis method [Fäh et al., 2009] was used to estimate the ellipticity function more accurately using the Matlab code of V. Poggi. In this method, the time-frequency analysis using the Wavelet transform is computed for each component. For each frequency, the maxima in time (10 per minute with at least $0.1\,\mathrm{s}$ between each) in the TFA are determined. The Horizontal to Vertical ratio of amplitudes for each maxima is then computed and statistical properties for each frequency are derived. The used wavelet is a Cosine wavelet with parameter 9. The mean of the distribution for each frequency is kept. For the sake of comparison, the time-frequency analysis by Fäh et al. [2001], based on the spectrogram, was also used, as well as the wavelet-based TFA coded in Geopsy.

The ellipticity extraction using the Capon analysis [Poggi and Fäh, 2010] on the array measurement was also performed (see section 5).

Method	Freq. band	Win. length	Anti-trig.	Overlap	Smoothing
Standard H/V Geopsy	$0.2 - 20\,\mathrm{Hz}$	$50\,\mathrm{s}$	No	50%	K&O 60
Standard H/V D. Fäh	$0.2 - 20\,\mathrm{Hz}$	$30\,\mathrm{s}$	No	75%	?
H/V TFA Geopsy	$0.2 - 20\,\mathrm{Hz}$	Morlet m=8 fi=1	No	-	?
H/V TFA D. Fäh	$0.2 - 20\,\mathrm{Hz}$	Specgram	No	-	?
H/V TFA V. Poggi	$0.2 - 20\,\mathrm{Hz}$	Cosine wpar=9	No	-	2D MA 10

Table 4: Methods and parameters used for the H/V processing.

4.2 Results in the array (Kloster)

H/V spectral ratios in the array are complex, especially in the central part of the array (Fig. 4). A low frequency bump can be recognized at $0.5\,\mathrm{Hz}$ but may be due to wind rather than to a deep resonance since it was not present on the temporary station previously installed in the building Klosterhof 7 (station XGAL1, Fig. 5). Only the first peak is picked. The fundamental frequency is found at $4\,\mathrm{Hz}$ at the STGK station site.

A North-South gradient is clearly observed: Points STG305 and 405 (light blue on Fig. 4) have only one clear peak at lower frequency at 3.5 and $2.8\,\mathrm{Hz}$, respectively, but it should be reminded that the signal may be filtered at high frequencies due to close buildings. The majority of points in the central part of the array (blue on Fig. 4) have first peak around $4\,\mathrm{Hz}$ and their

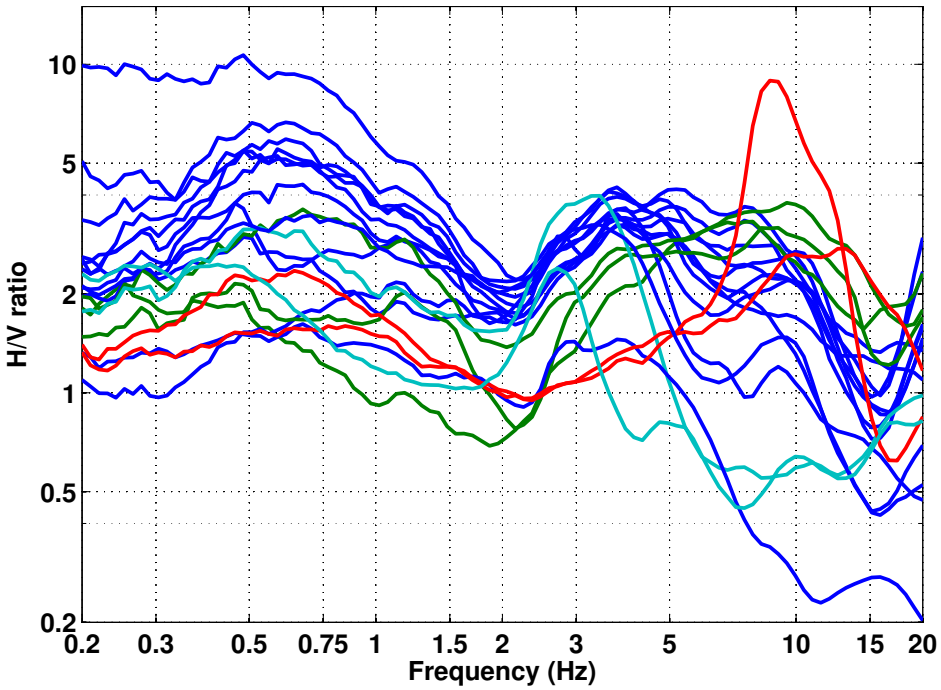

Figure 4: H/V spectral ratios (time-frequency analysis code V. Poggi). Colors stand for the 4 categories of points described in the text.

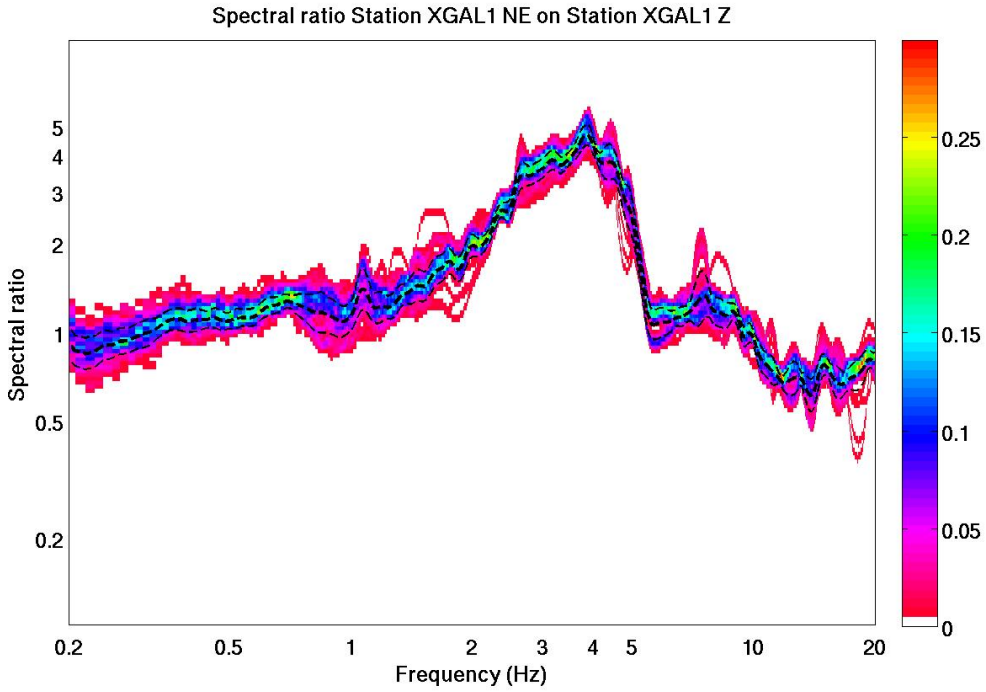

Figure 5: H/V spectral ratios on long recording at station XGAL1, located at the station STGK site.

right flank is well defined above $8\,\mathrm{Hz}$, but they also show high frequency peaks up to $10\,\mathrm{Hz}$ (broad range of high amplitudes). Points 203, 302 and 303 (green on Fig. 4), in the southern part of the Kloster, are intermediate with unclear peaks around $4\,\mathrm{Hz}$ and clearer peaks at high frequency around $10\,\mathrm{Hz}$. Finally, points 402 and 403 (red on Fig. 4), the most to the South, have their first and only peak at high frequency at $9 - 10\,\mathrm{Hz}$.
This can be interpreted as a major layer resonating in the Northern and central part with increasing depth to the North (disappearing south of the Kloster), as well as other surface layers under the Kloster and to the South. Therefore, the peak frequency cannot be interpreted directly as the bedrock depth since it represents different layers.

Moreover, all the methods to compute H/V ratios are compared on Fig. 7, where the classical methods were divided by $\sqrt{2}$ to correct from Love waves influence [Fäh et al., 2001]. Ellipticity from the 3C FK analysis is shifted towards higher frequencies compared to the ellipticity at the central point computed with the other methods due to the variability in the array. It should be noticed that most of the noise sources is due to the road, located southern from the array, where the H/V peak is at higher frequency.

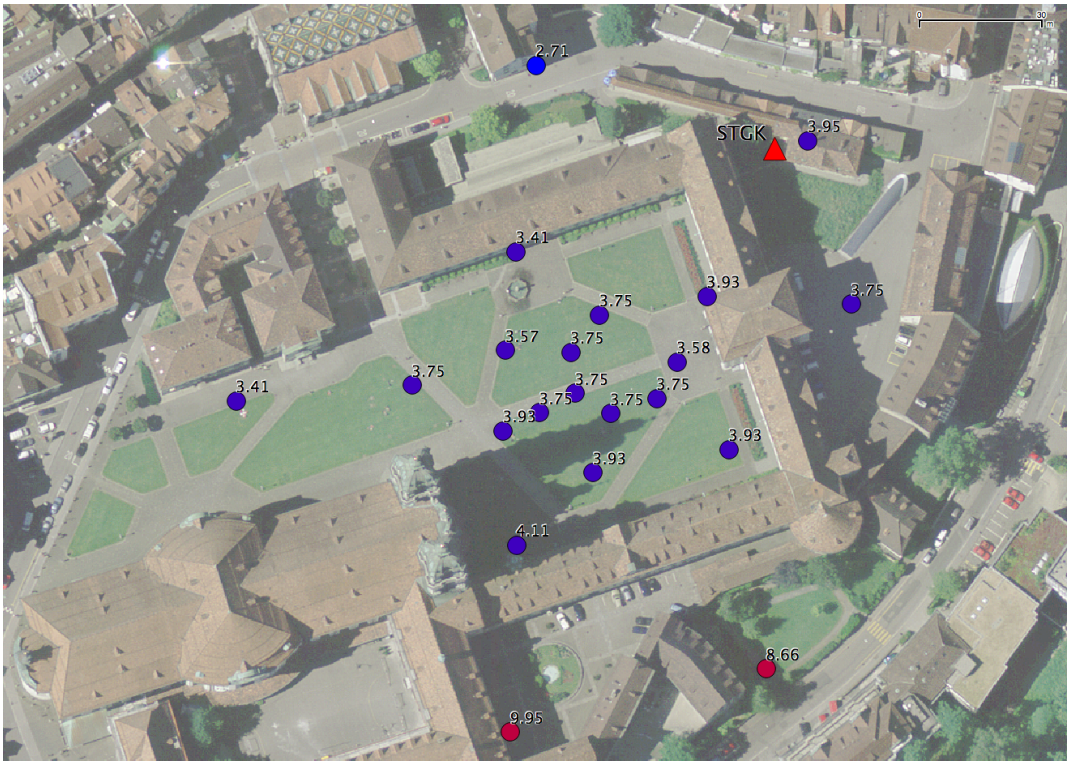

Figure 6: H/V frequency map around the array.

4.3 Results in the whole city

Fig. 8 shows the maps of the fundamental frequencies derived from the H/V curves of the recordings. The basin shape, correlated at the first order with the resonance frequency, is clearly visible. Its lateral variations are rapid. The peak frequency is minimum in the centre of the basin, at the "Stadtpark", with a value of $2.4\,\mathrm{Hz}$, but most of the values are around $3 - 4\,\mathrm{Hz}$, up

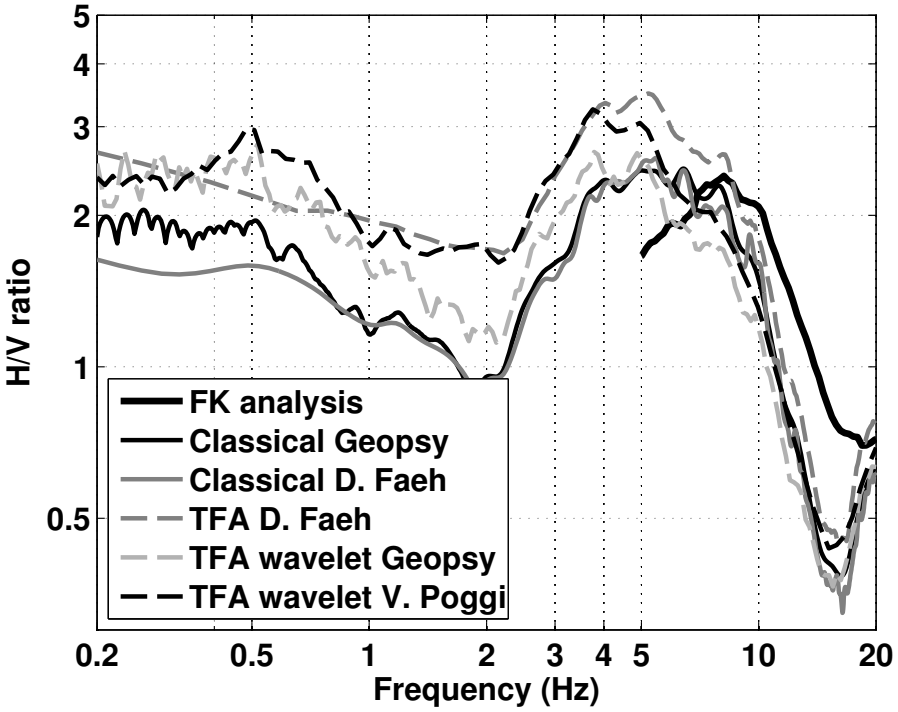

Figure 7: H/V spectral ratios for point STG000 using the different codes. Classical methods were divided by $\sqrt{2}$.

to $10 - 15$ Hz in the surrounding slopes. No characteristic makes the old city different from the rest of the city: it is built in the basin probably on better quality surface layers, but no difference can be noticed in depth.

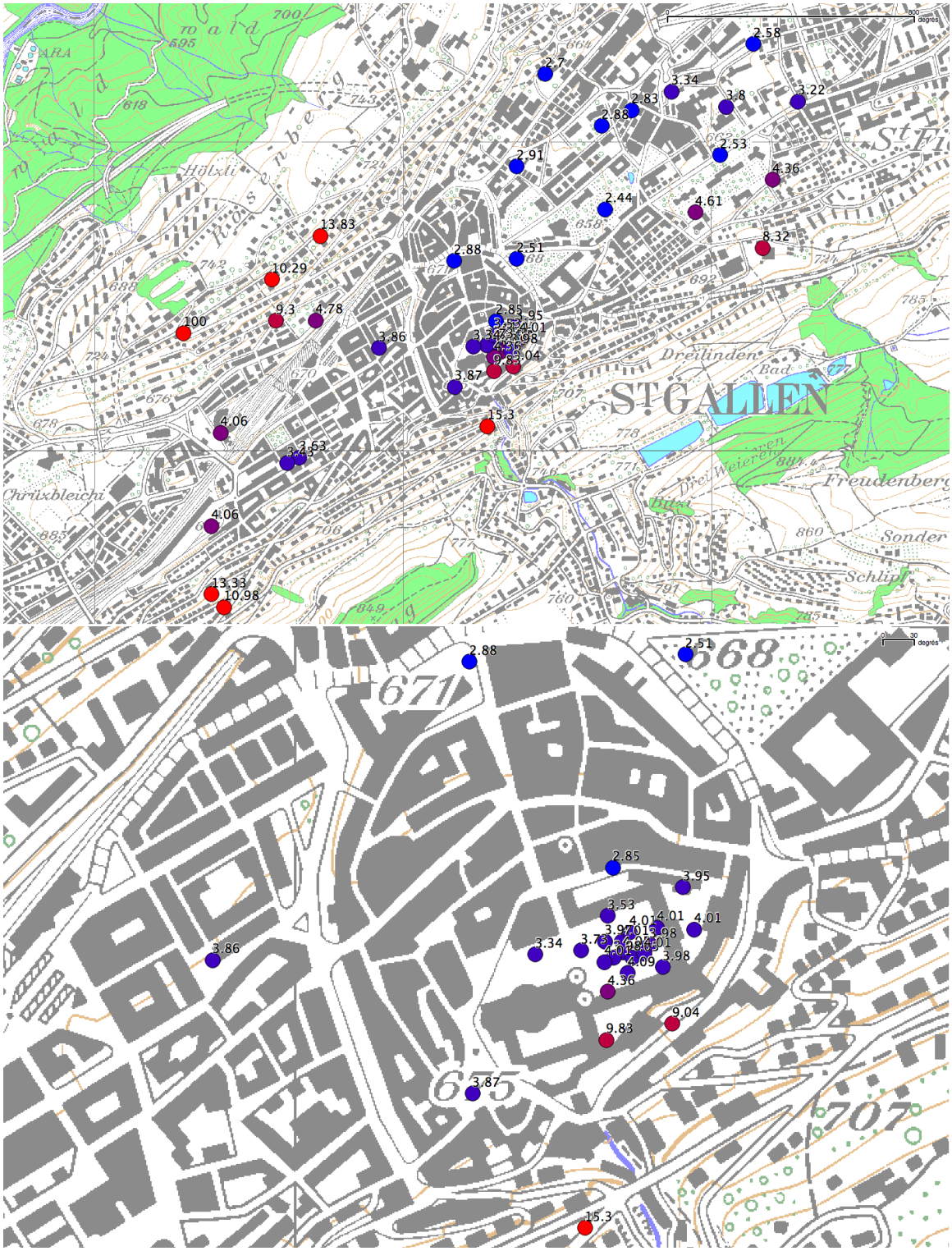

Figure 8: H/V frequency map of the whole city (top) and zoom on the old town (bottom).

5 Array processing

5.1 Processing methods and parameters

The vertical components of the arrays were processed using the High-resolution FK analysis [Capon, 1969] using the Geopsy `http://www.geopsy.org` software. Large time windows were considered (300T) because it provided better results. The results of computations of both datasets were merged to estimate the dispersion curves.

Moreover, a 3C array analysis [Fäh et al., 2008] was also performed using the array_tool_3C software [Poggi and Fäh, 2010]. It allows to derive Rayleigh and Love modes. The results of computations of both datasets were merged to estimate the dispersion curves. However, the second configuration does not bring information on the Rayleigh modes.

The array was also processed following the method proposed in Maranò et al. [2012]. Results are obtained jointly modeling up to three propagating plane waves at each time window and frequency. The method models both Rayleigh and Love waves. The recording is split in windows of 20 seconds. Parameter estimation is done via maximum likelihood considering jointly all the measurement from three components sensors. Wavefield parameters estimated include wavenumber, azimuth, and Rayleigh wave ellipticity. Model selection (choice of wave type and number of waves) is performed using the Bayesian information criterion.

Dataset 2 does not provide good results, except on the transverse component. However, results of both datasets are consistent, which is not obvious considering the large H/V variation across the array.

Method	Set	Freq. band	Win. length	Anti-trig.	Overlap	Grid step	Grid size	# max.
HRFK 1C	1	$2-25$ Hz	$300T$	No	50%	0.001	0.7	5
HRFK 1C	2	$2-25$ Hz	$300T$	No	50%	0.001	0.7	5
HRFK 3C	1	$2-25$ Hz	Wav. 10 Tap. 0.2	No	50%	150 m/s	3000 m/s	5
HRFK 3C	2	$2-25$ Hz	Wav. 10 Tap. 0.2	No	50%	150 m/s	3000 m/s	5
Wavef. dec.	1&2	$1-20$ Hz	20s					

Table 5: Methods and parameters used for the array processing.

5.2 Obtained dispersion curves

In the vertical direction in the 1C FK analysis, a dispersion curve can be picked between 5 and 15 Hz (Fig. 9) including its standard deviation. The velocities are ranging from $1500\,\mathrm{m/s}$ at 5 Hz down to $350\,\mathrm{m/s}$ at 15 Hz.

Using the 3C analysis, vertical, radial and transverse directions allow to pick 3 different curves (Fig. 9), the radial curve being exactly in between the Rayleigh and Love modes. It should be noticed that using original or rotated recordings lead to exactly the same results in the 3 directions. Moreover, a test without point STG305, contaminated by soil-structure

interaction, does also lead to the same results. The vertical direction shows little difference with the 1C analysis (Fig. 11) below $8\,\mathrm{Hz}$. It should however be noticed that this results only from the first dataset, therefore implying a higher frequency value for the array limit ($6.8\,\mathrm{Hz}$ instead of $5.2\,\mathrm{Hz}$ for the second dataset). Love fundamental mode can also be picked from 5 to $15\,\mathrm{Hz}$ in the transverse direction with velocities of $200\,\mathrm{m/s}$ at $15\,\mathrm{Hz}$.

The final selection is displayed on Fig. 12.

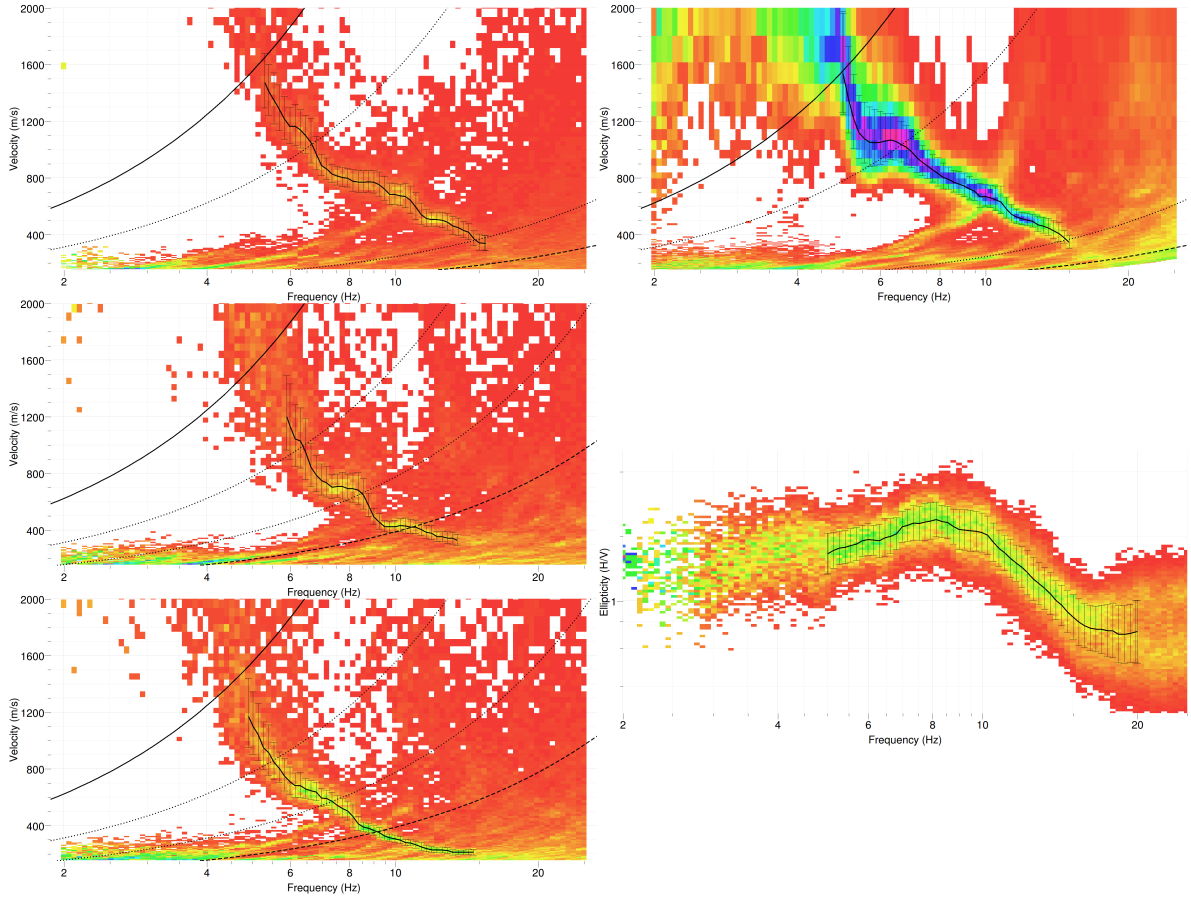

Figure 9: Dispersion curve obtained from the 3C (left) and the 1C (top right) array analysis in the vertical (top), radial (centre) and transverse (bottom) directions and ellipticity (bottom right) obtained from the 3C analysis.

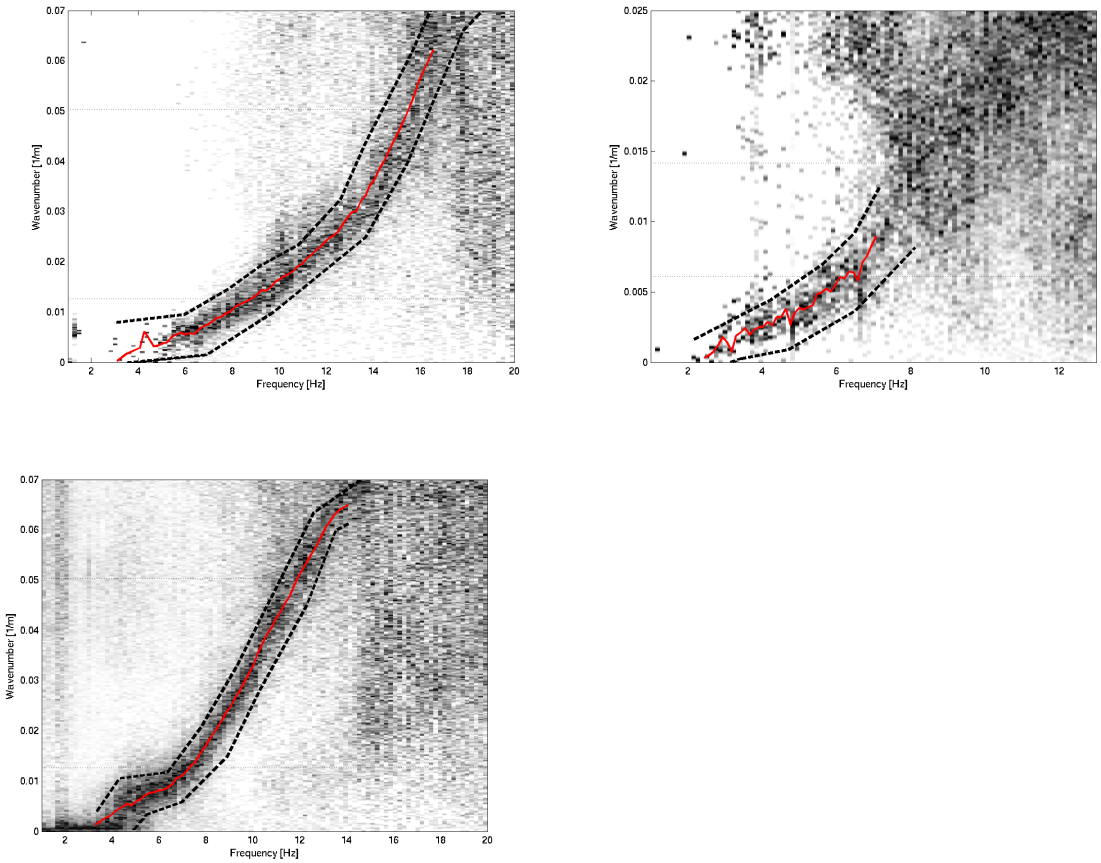

Figure 10: Dispersion picking using the Maranò et al. [2012] method. Top: Rayleigh; Bottom: Love; Left: dataset 1; Right: dataset 2.

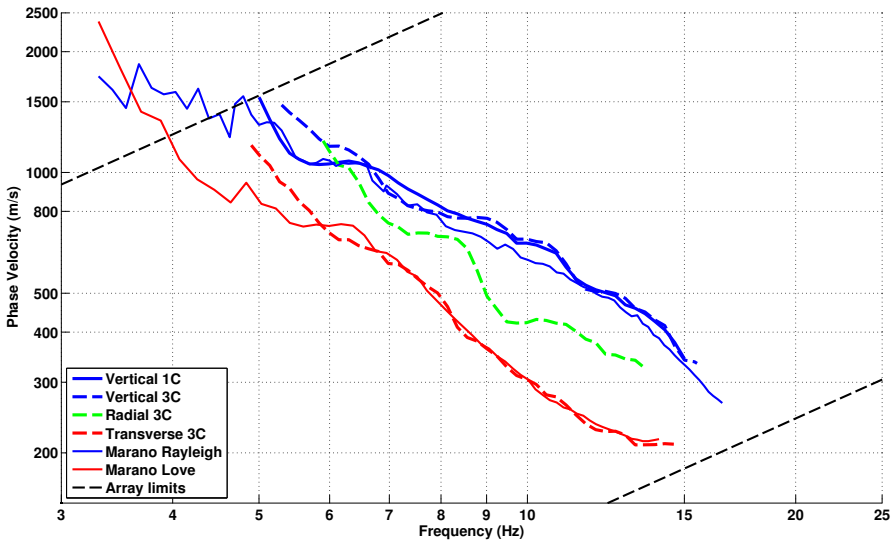

Figure 11: Picked dispersion curves from 1C, 3C analyses and wavefield decomposition.

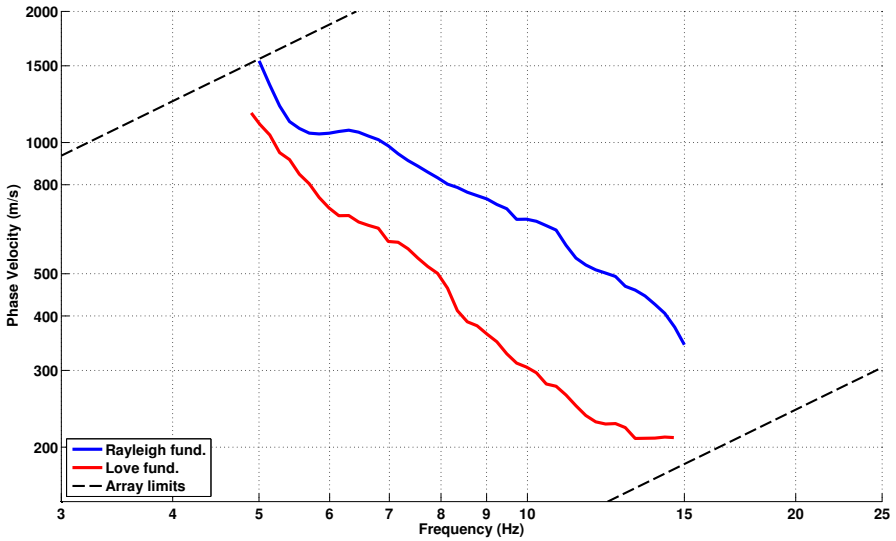

Figure 12: Selected dispersion curves.

6 Inversion and derived parameters

6.1 Inversion

For the inversion, the selected dispersion curves were used as simultaneous targets without standard deviation to avoid different weighting. The ellipticity information was not used and is displayed in the following for comparison only. All curves were resampled using 50 points between 2 and 20 Hz in log scale.

The inversion was performed using the Improved Neighborhood Algorithm (NA) [Wathelet, 2008] implemented in the Dinver software. In this algorithm, the tuning parameters are the following: Ns_0 is the number of starting models, randomly distributed in the parameter space, Nr is the the number of best cells considered around these Ns_0 models, Ns is the number of new cells generated in the neighborhood of the Nr cells (Ns/Nr per cell) and It_{max} is the number of iteration of this process. The process ends with $Ns_0 + Nr * \frac{Ns}{Nr} * It_{max}$ models. The used parameters are detailed in Tab. 6.

It_{max}	Ns_0	Ns	Nr
500	10000	100	100

Table 6: Tuning parameters of Neighborhood Algorithm.

During the inversion process, low velocity zones were not allowed. The Poisson ratio was inverted in each layer in the range 0.2-0.45 and the density was supposed equal to $2000\,\mathrm{kg/m^3}$ except for the layers assumed to be rock ($2500\,\mathrm{kg/m^3}$). Inversions with free layer depths as well as fixed layer depths were performed. Increasing number of layers are used to smooth the obtained results and better explore the parameter space. 5 independent runs of 5 different parametrization schemes (5 and 6 layers over a half space and 11, 13 and 15 layers with fixed depth) were performed. For further elaborations, the best models of these 25 runs were selected (Fig. 15).

The velocity profiles indicate a low velocity on the first $5 - 8\,\mathrm{m}$, between 100 and $300\,\mathrm{m/s}$. Until 12 to $20\,\mathrm{m}$, the velocity is around $500 - 600\,\mathrm{m/s}$, which likely corresponds to moraine. At this depth, an interface is found with a velocity of the lower layer reaching $800\,\mathrm{m/s}$. Below, the velocity increases slowly with depth, up to approximately $1200\,\mathrm{m/s}$. The moraine/rock interface, is however poorly constrained between 35 and $45\,\mathrm{m}$ depth. Some inversions even don't show any interface (fixed layer depth), showing a velocity increase down to the maximum allowed depth. The velocity in the bedrock seems to converge to $1600\,\mathrm{m/s}$ although it is probably badly constrained.

When compared to the target curves (Fig. 13), the Love and Rayleigh modes are reproduced. The ellipticity that is not used in the inversion, however, is much more complex in the data than what is produced by the model. The upper part is therefore well constrained by the dispersion curves but the confidence in the depth moraine/molasse interface is therefore low.

Assuming the topographic slope of the molasse remains constant below the sediments ($14\,^\circ$ from the Swisstopo map), the sediments thickness is found to be around $35\,\mathrm{m}$ at the centre of

the array, which is compatible with these results. The same computation gives around $40\,\mathrm{m}$ for the station STGK.

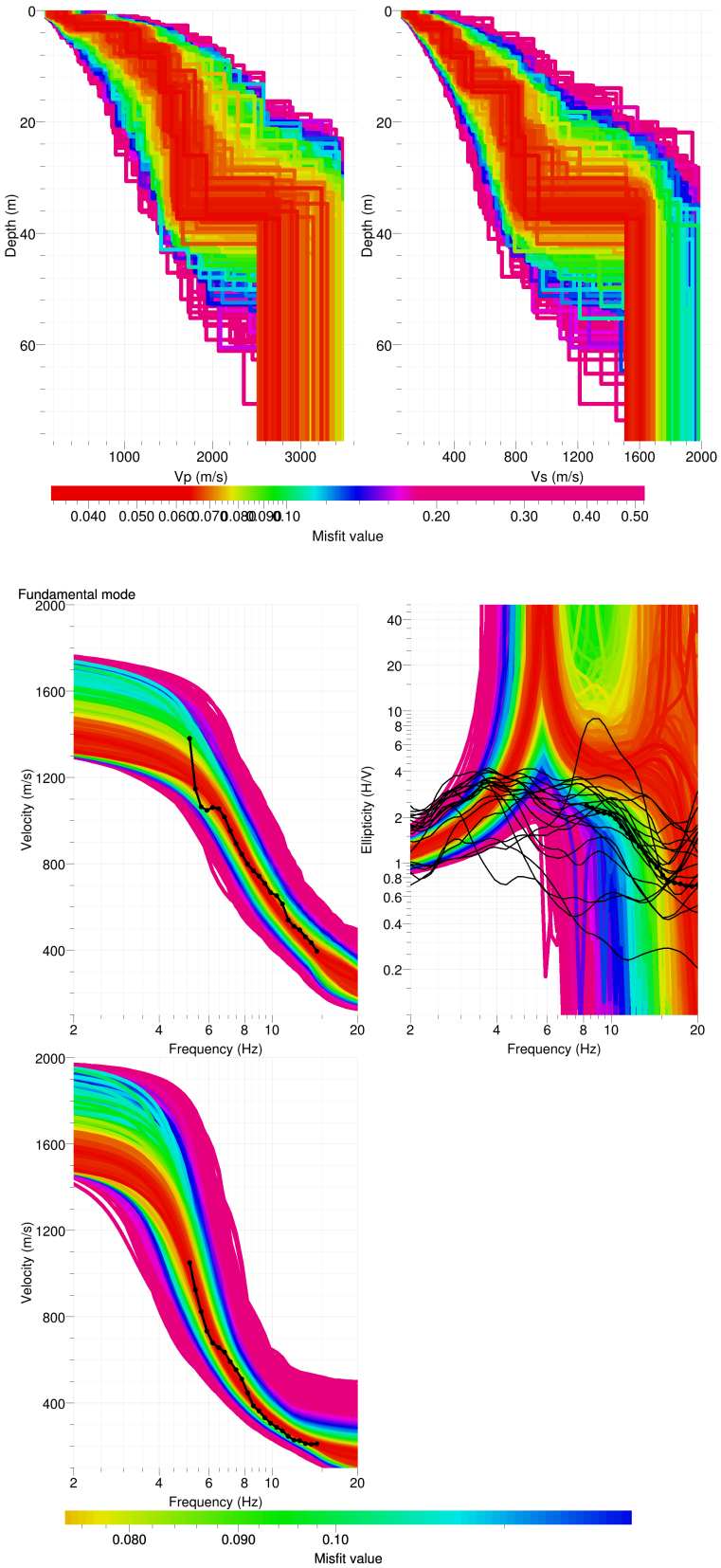

Figure 13: Inverted ground profiles in terms of V_p and V_s (top) and comparison between inverted models and measured Rayleigh and Love modes and corresponding ellipticity, free layer depth strategy.

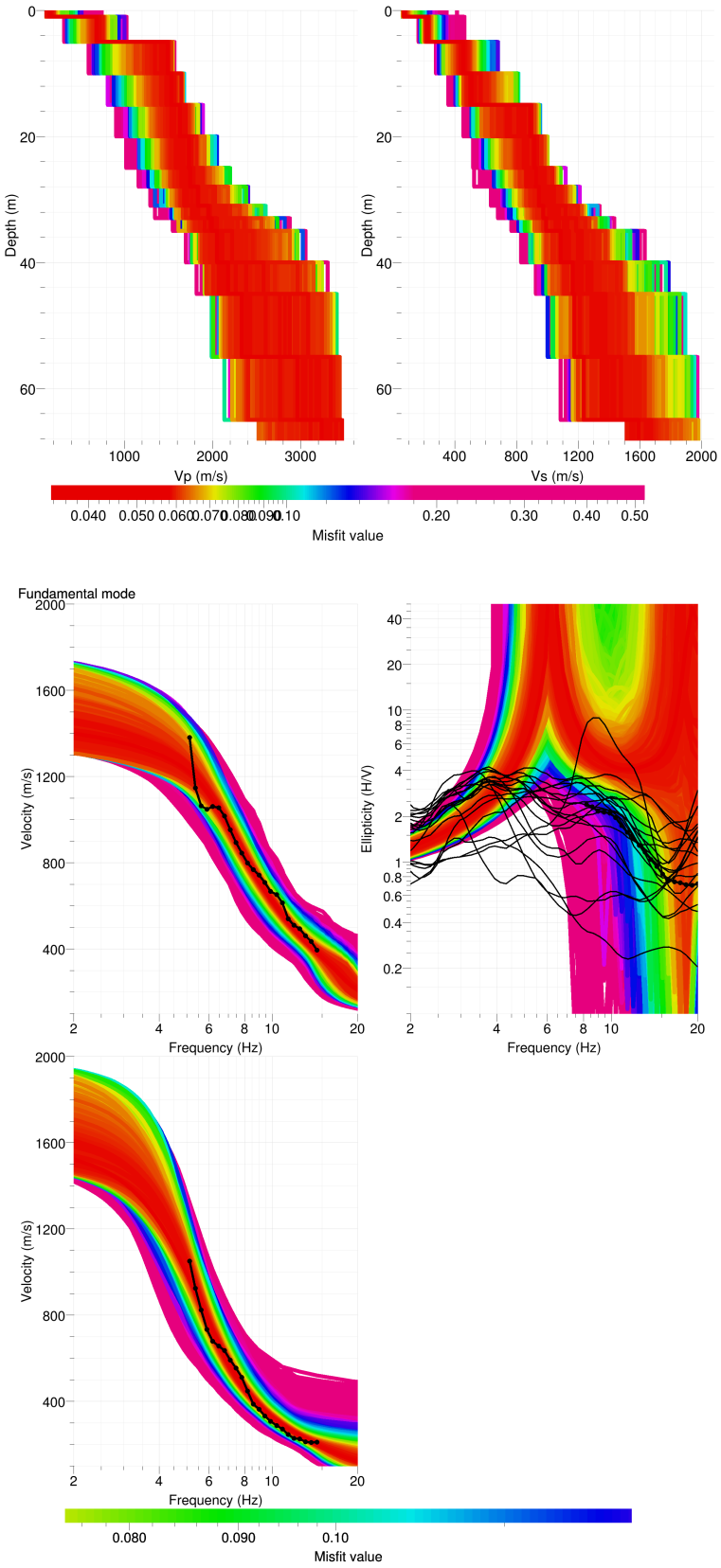

Figure 14: Inverted ground profiles in terms of V_p and V_s (top) and comparison between inverted models and measured Rayleigh and Love modes and corresponding ellipticity, fixed layer depth strategy.

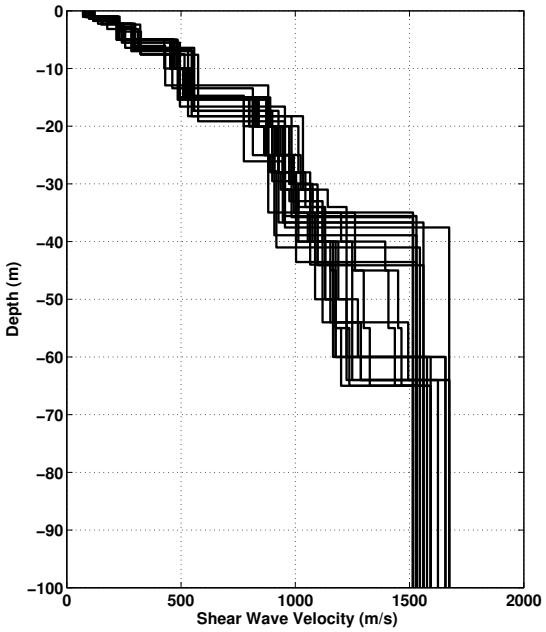

Figure 15: V_s ground profiles for the selected 25 best models.

6.2 Travel time average velocities and ground type

The distribution of the travel time average velocities at different depths was computed from the selected models. The uncertainty, computed as the standard deviation of the distribution of travel time average velocities for the considered models, is also provided, but its meaning is doubtful. $V_{s,30}$ is found to be $440\,\mathrm{m/s}$. Considering the first $15\,\mathrm{m}$ with a velocity around $100 - 500\,\mathrm{m/s}$) and velocity below $15\,\mathrm{m}$ being $800\,\mathrm{m/s}$, the site can be classified as class E in the SIA261 [SIA, 2003], whereas the contrast is not strong enough for Eurocode 8 [CEN, 2004], where it would be classified in class B.

	Mean (m/s)	**Uncertainty (m/s)**
$V_{s,5}$	166	10
$V_{s,10}$	241	7
$V_{s,20}$	348	6
$V_{s,30}$	440	7
$V_{s,40}$	514	7
$V_{s,50}$	577	8
$V_{s,100}$	-	-
$V_{s,150}$	-	-
$V_{s,200}$	-	-

Table 7: Travel time averages at different depths from the inverted models. Uncertainty is given as one standard deviation from the selected profiles.

6.3 SH transfer function and quarter-wavelength velocity

The quarter-wavelength velocity approach [Joyner et al., 1981] provides, for a given frequency, the average velocity at a depth corresponding to 1/4 of the wavelength of interest. It is useful to identify the frequency limits of the experimental data (minimum frequency in ellipticity and dispersion curves, $5\,\mathrm{Hz}$ here). The results using this proxy show that no data is controlling the results below $13\,\mathrm{m}$ (Fig. 16). Moreover, the quarter wavelength impedance-contrast introduced by Poggi et al. [2012] is also displayed in the figure. It corresponds to the ratio between two quarter-wavelength average velocities, respectively from the top and the bottom part of the velocity profile, at a given frequency [Poggi et al., 2012]. It shows a trough (inverse shows a peak) at the resonance frequency.
Moreover, the theoretical SH-wave transfer function for vertical propagation [Roesset, 1970] is computed from the inverted profiles. It is compared to the quarter-wavelength amplification [Joyner et al., 1981], that however cannot take resonances into account (Fig. 17). In this case, the models are predicting an amplification of a factor of 5 at a $5\,\mathrm{Hz}$ frequency, increasing for high frequencies. This will be compared to observations at this station.

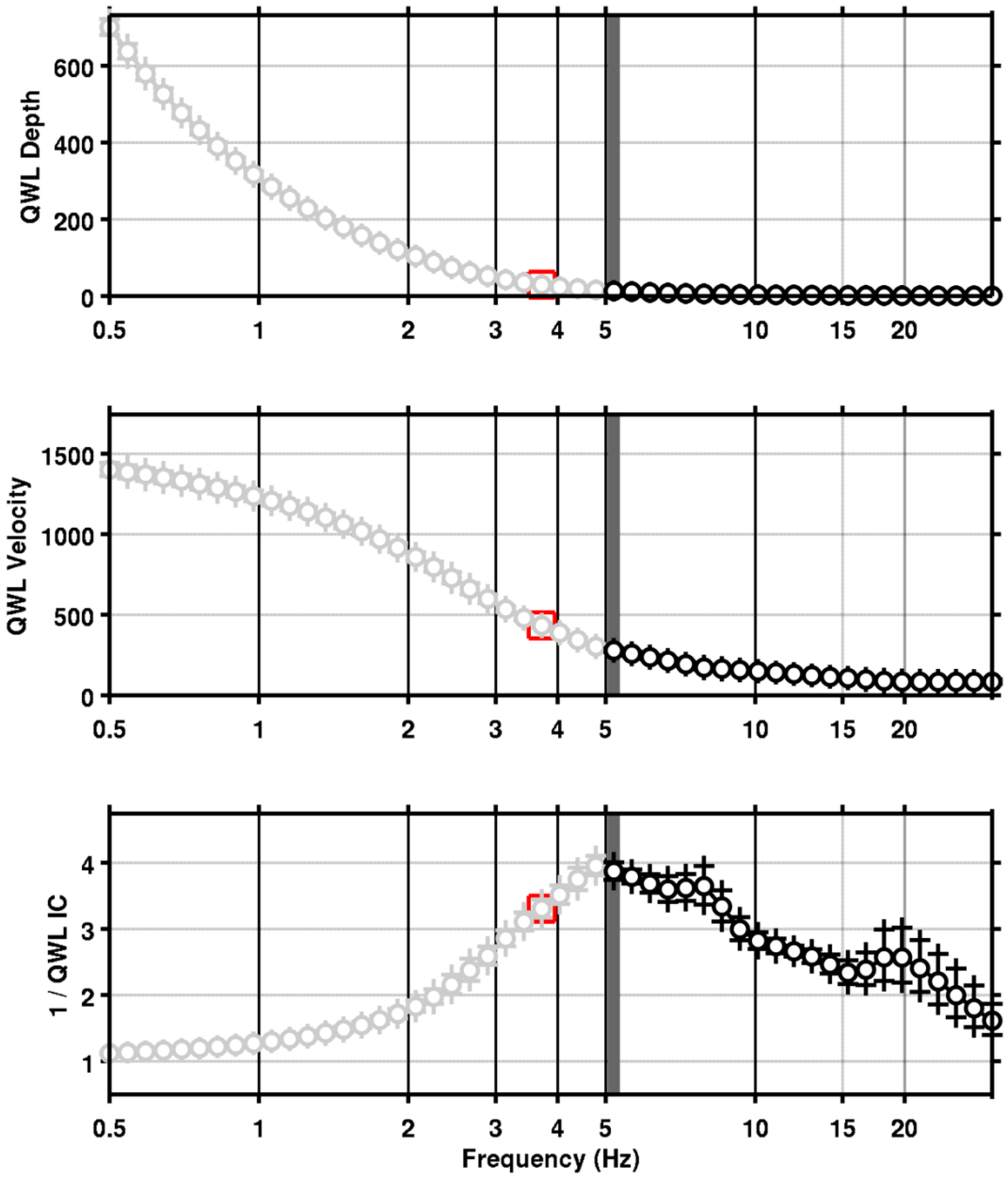

Figure 16: Quarter wavelength velocity representation of the velocity profile (top: depth, centre: velocity, bottom: inverse of the impedance contrast). Black curve is constrained by the dispersion curves, light grey is not constrained by the data. Red square is corresponding to $V_{s,30}$.

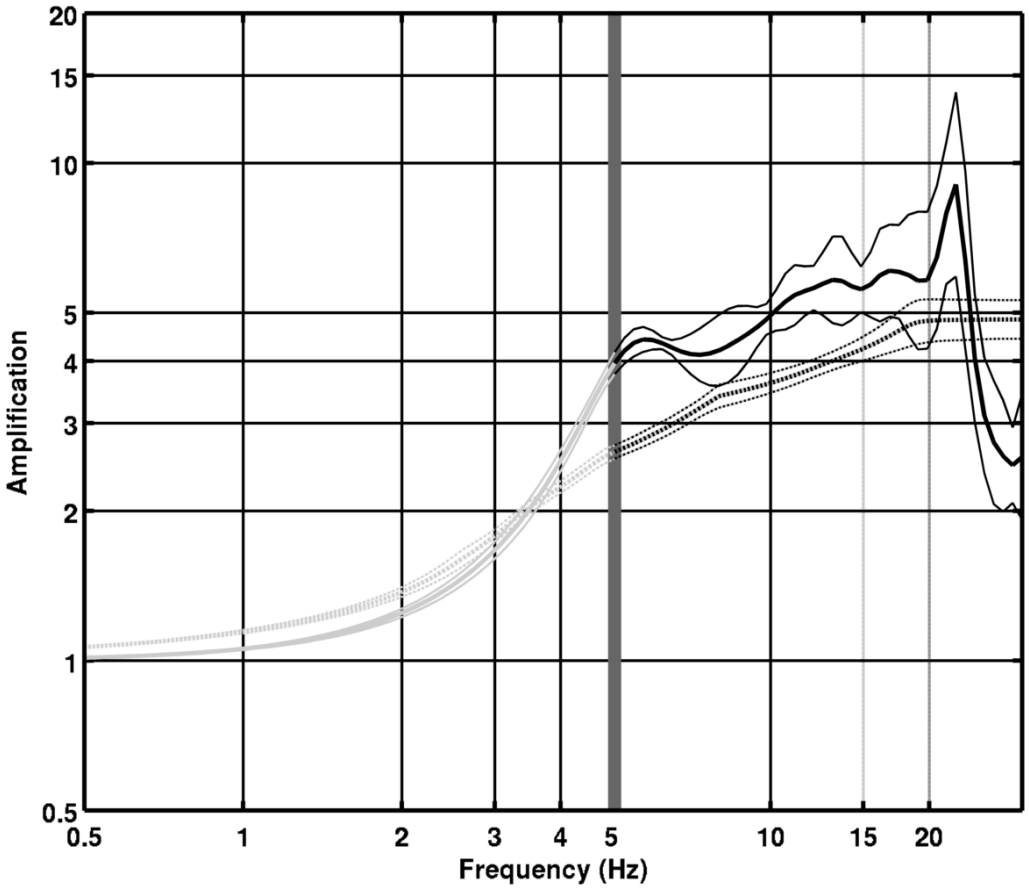

Figure 17: Theoretical SH transfer function (solid line) and quarter wavelength impedance contrast (dashed line) with their standard deviation. Significance of the greyshades is detailed in Fig. 16.

7 Interpretation

The geophysical data collected in St Gallen together with borehole data provided by the Kantonsamt für Umwelt und Energie (number in the archive: 7904 - not displayed here for confidentiality reasons) allowed to interpret the soil column below station STGK (Fig. 18). The borehole shows $4\,\mathrm{m}$ of human infill, $6.4\,\mathrm{m}$ of fluvio-lacustrine sediments (more or less silty sands with gravels). Below $10.4\,\mathrm{m}$, weathered moraine is found. Other boreholes, located couple of meters away to the South-East show a quite different picture without fluvio-lacustrine sediments (moraine at $2\,\mathrm{m}$ depth). Finally, a last borehole located in the Northern part of the array, shows $2.7\,\mathrm{m}$ of human infill, $17.3\,\mathrm{m}$ of fluvio-lacustrine sediments (more or less silty sands with gravels), and moraine at $20\,\mathrm{m}$ depth. As a conclusion, it a large variability is noticed in the depth of the different layers, within the array size, as already remarked from the H/V data.

The interpretation of the inverted profiles is as follows. The upper $1-2\,\mathrm{m}$, made of human infill (mostly fine sand) are weak with a shear wave velocity of $100\,\mathrm{m/s}$. An intermediate layer, down to 5 to $8\,\mathrm{m}$, is made of fluvio-glacial silt sediments, with a velocity of $200-300\,\mathrm{m/s}$. Below $8\,\mathrm{m}$, one finds the moraine with a velocity first of $500\,\mathrm{m/s}$ (weathered moraine) and then close to $800\,\mathrm{m/s}$ at $12-20\,\mathrm{m}$. Finally the moraine/molasse interface is not well constrained at an estimated depth of $40\,\mathrm{m}$ at STGK. The molasse has a velocity of about $1500\,\mathrm{m/s}$.

The major issue in this inversion is the ellipticity. First, it is clear that the lateral variability is high and that the ellipticity can be highly variable as well. The inversion however all lead to a $6\,\mathrm{Hz}$ clear peak that is associated in the profiles to the interface between weathered moraine and hard moraine. In XGAL1 station (test station in the house close to STGK) and in STG401 (closest array station to STGK), such a high frequency peak is not present (Fig. 18). This figure shows different curves that could serve as proxy for the H/V at STGK station. The red curve is obtained by using the STGK accelerometric data and is therefore biased at low frequencies (noise of the sensor). The green curve is the closest recording to STGK during the array measurement but is surprisingly low amplitude. Finally, the orange curve comes from XGAL1, which is the most reliable proxy, although differences with STGK can be noticed above $6\,\mathrm{Hz}$ because XGAL1 is not in the free field. It shows how variable the H/V ratios can be over short distances.

An interpretation of the H/V curve could be that the lowest frequency peak around $4\,\mathrm{Hz}$ at STGK, and varying in the city as shown in the H/V analysis is produced by the contrast between the moraine and the molasse. This interface is not present in the Southern part of the array, where the weak sediments (less deep) are directly in contact with the bedrock.

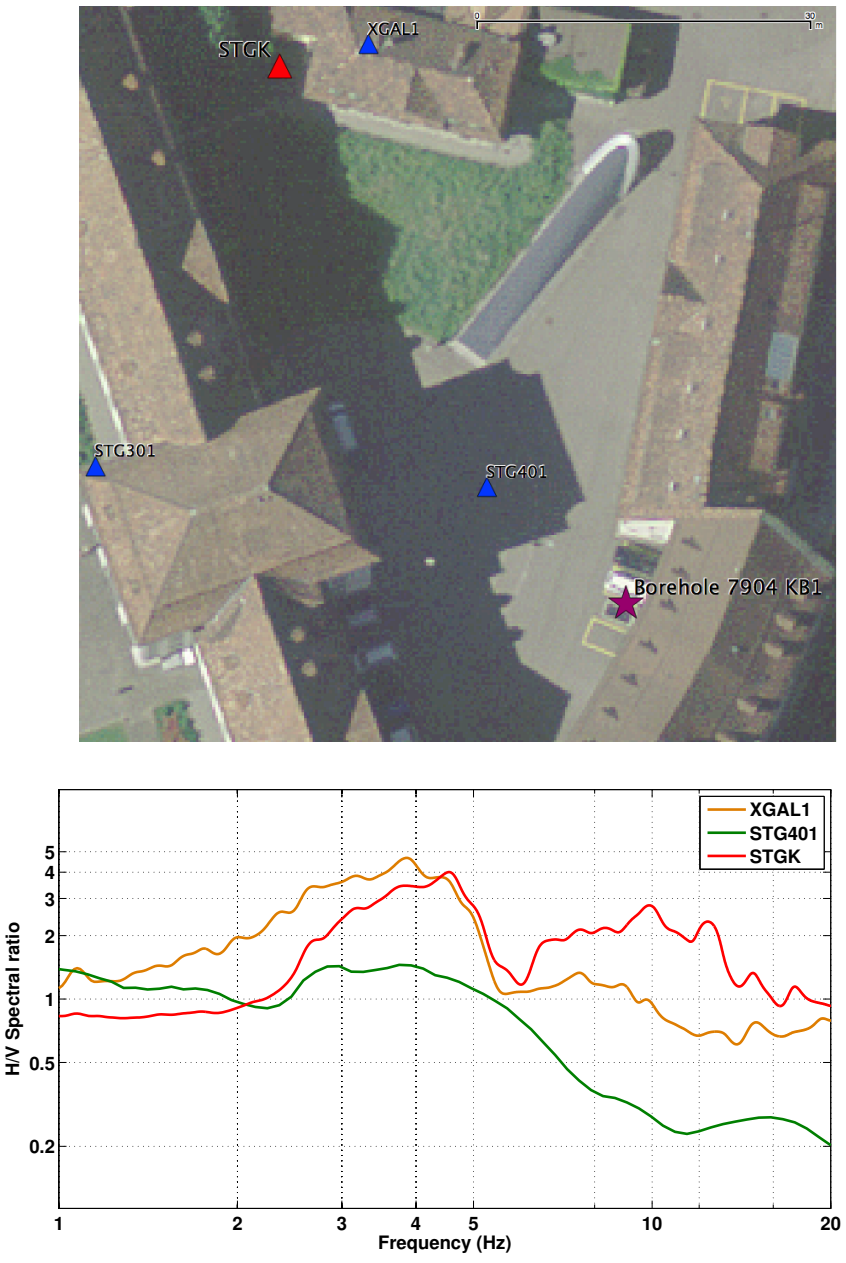

Figure 18: H/V spectral ratios for STGK station.

8 Conclusion

This study used ambient vibration array measurements to derive a velocity model for station STGK. Basic assumptions of array analysis were not fulfilled, including a strong lateral variability. Especially, ellipticity information was not robust enough to constrain the inversion. The results agree with borehole data but these models may be revised in the future, when more data will be available.

Moreover, a H/V survey allowed to map the fundamental frequency below St Gallen city. Because of the lateral variability of the different layers, interpreting this frequency in terms of bedrock depth is however difficult.

At STGK site, $V_{s,30}$ is found to be close to $440\,\mathrm{m/s}$, and the site class is B in EC8 and E in SIA261. The theoretical SH transfer function and impedance contrast of the quarter-wavelength velocity computed from the inverted profiles support a large amplification above $5\,\mathrm{Hz}$.

Acknowledgements

The authors thank Ivo Egger and Andreas Stutz who performed the single station measurements, Valentin Gischig for the help during the array measurements, as well as Daniel Gilgen and Franz Weber for the design of the realtime system.

References

Sylvette Bonnefoy-Claudet, Fabrice Cotton, and Pierre-Yves Bard. The nature of noise wavefield and its applications for site effects studies. *Earth-Science Reviews*, 79(3-4): 205–227, December 2006. ISSN 00128252. doi: 10.1016/j.earscirev.2006.07.004. URL http://linkinghub.elsevier.com/retrieve/pii/S0012825206001012.

J M.W Brownjohn, A Pavic, and P Omenzetter. A spectral density approach for modelling continuous vertical forces on pedestrian structures due to walking. *Canadian Journal of Civil Engineering*, 31(1):65–77, January 2004. ISSN 0315-1468. doi: 10.1139/l03-072. URL http://www.nrcresearchpress.com/doi/abs/10.1139/l03-072.

J. Capon. High-Resolution Frequency-Wavenumber Spectrum Analysis. *Proceedings of the IEEE*, 57(8):1408–1418, 1969.

CEN. *Eurocode 8: Design of structures for earthquake resistance - Part 1: General rules, seismic actions and rules for buildings*. European Committee for Standardization, en 1998-1: edition, 2004.

Donat Fäh, Fortunat Kind, and Domenico Giardini. A theoretical investigation of average H / V ratios. *Geophysical Journal International*, 145:535–549, 2001.

Donat Fäh, Gabriela Stamm, and Hans-Balder Havenith. Analysis of three-component ambient vibration array measurements. *Geophysical Journal International*, 172(1):199–213, January 2008. ISSN 0956540X. doi: 10.1111/j.1365-246X.2007.03625.x. URL http://doi.wiley.com/10.1111/j.1365-246X.2007.03625.x.

Donat Fäh, Marc Wathelet, Miriam Kristekova, Hans-Balder Havenith, Brigitte Endrun, Gabriela Stamm, Valerio Poggi, Jan Burjanek, and Cécile Cornou. Using Ellipticity Information for Site Characterisation Using Ellipticity Information for Site Characterisation. Technical report, NERIES JRA4 Task B2, 2009.

William B. Joyner, Richard E. Warrick, and Thomas E. Fumal. The effect of Quaternary alluvium on strong ground motion in the Coyote Lake, California, earthquake of 1979. *Bulletin of the Seismological Society of America*, 71(4):1333–1349, 1981.

Katsuaki Konno and Tatsuo Ohmachi. Ground-Motion Characteristics Estimated from Spectral Ratio between Horizontal and Vertical Components of Microtremor. *Bulletin of the Seismological Society of America*, 88(1):228–241, 1998.

Stefano Maranò, C. Reller, H.-A. Loeliger, and Donat Fäh. Seismic waves estimation and wave field decomposition: Application to ambient vibrations. *Geophysical Journal International*, submitted, 2012.

Valerio Poggi and Donat Fäh. Estimating Rayleigh wave particle motion from three-component array analysis of ambient vibrations. *Geophysical Journal International*, 180(1):251–267, January 2010. ISSN 0956540X. doi: 10.1111/j.1365-246X.2009.04402.x. URL http://doi.wiley.com/10.1111/j.1365-246X.2009.04402.x.

Valerio Poggi, Benjamin Edwards, and Donat Fäh. Characterizing the Vertical-to-Horizontal Ratio of Ground Motion at Soft Sediment-Sites. *Bulletin of the Seismological Society of America*, 102(6), 2012. doi: 10.1785/0120120039.

J.M. Roesset. Fundamentals of soil amplification. In R. J. Hansen, editor, *Seismic Design for Nuclear Power Plants*, pages 183–244. M.I.T. Press, Cambridge, Mass., 1970. ISBN 978-0-262-08041-5. URL `http://mitpress.mit.edu/catalog/item/default.asp?ttype=2\&tid=5998`.

SIA. *SIA 261 Actions sur les structures porteuses*. Société suisse des ingénieurs et des architectes, Zürich, sia 261:20 edition, 2003.

Marc Wathelet. An improved neighborhood algorithm: Parameter conditions and dynamic scaling. *Geophysical Research Letters*, 35(9):1–5, May 2008. ISSN 0094-8276. doi: 10.1029/2008GL033256. URL `http://www.agu.org/pubs/crossref/2008/2008GL033256.shtml`.